

Contents lists available at ScienceDirect

Cement and Concrete Composites

journal homepage: www.elsevier.com/locate/cemconcomp





A comparative investigation on the effects of nanocellulose from bacteria and plant-based sources for cementitious composites

Muhammad Intesarul Haque, Warda Ashraf*, Rakibul I. Khan, Surendra Shah

Department of Civil Engineering, Center for Advanced Construction Materials (CACM), University of Texas at Arlington, Nedderman Hall, Arlington, TX, 76010, USA

ARTICLE INFO

Keywords:
Cellulose nanofibrils
Bacterial cellulose
Strength
Alkali silica reaction (ASR)
Mercury intrusion porosimeter (MIP)
Nanoindentation

ABSTRACT

Interest in cellulosic nanomaterials has recently gained momentum due to their high tensile strength and hygroscopic properties. This study compared the effects of two different types of cellulose nanomaterials, including cellulose nanofibrils (CNF) produced from wood and bacterial cellulose (BC), on the macro, micro, and nano scale performances of Ordinary Portland Cement (OPC) paste. Effects of CNF and BC on cement paste hydration, microstructure, compressive strength, and flexural strength were monitored. Four dosages of nanocellulose (0%, 0.05%, 0.1% and 0.3%, by weight) were used to prepare cement paste samples. Both CNF and BC were found to increase compressive strengths and flexural strengths by 10% and 55%, respectively, after 90 days of curing. However, only CNF was able to suppress the expansion of mortar samples due to the alkali-silica reaction by 33%. At the microscale, CNF was found to accelerate the early age cement hydration, whereas BC delayed cement hydration. Both nanocellulose types resulted in lower calcium hydroxide (CH) and higher CSH contents compared to the control batch after long-term curing. Statistical nanoindentations showed that the additions of nanocellulose increase the relative amounts of high-density CSH in the hydrated cement paste. The mercury intrusion porosimeter (MIP) and dynamic vapor sorption (DVS) analyses indicated that both types of nanocellulose increase the nanoporosity and reduced the microporosity. However, such advantages were more prominent in the case of CNF compared to the BC.

1. Introduction

Bio-based nanomaterials, including nanocellulose, have recently attracted significant research interest because of their great potential for producing a variety of high-value composites with low environmental impacts [1]. A fairly considerable amount of work involving cellulose in cement-based composites has already been published [2]. Cellulose is the most widely available organic compound on Earth [3]. It can be obtained from different sources like plants, animals, and bacteria. Cellulose is a chain-shaped molecule which contains 14,000 units of D-glucose held by hydrogen bonding [4,5]. Conventionally, cellulose microfibers are used in cement-based composites as reinforcing ingredients [2,6]. Due to its high specific surface area and superior mechanical properties [7] blended with the unique features of nanomaterials [8], nanocellulose can also significantly enhance the properties of concrete. Previous studies have shown that the addition of nanocellulose can control plastic shrinkage and increase the strength of concrete [9,10]. Additionally, the use of nanocellulose fibers can prevent the growth and propagation of cracks in cementitious composites

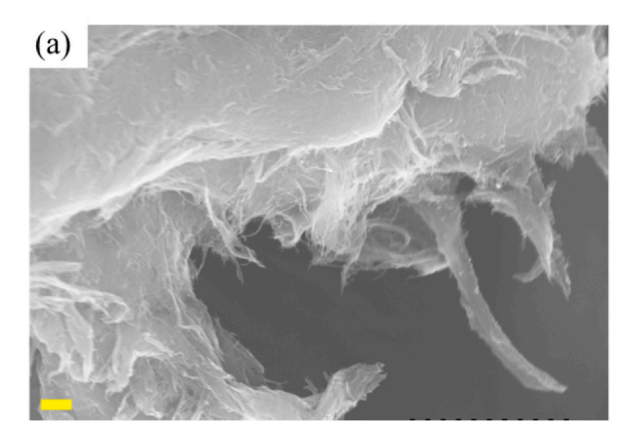
[11-13].

There are two alternative routes to synthesize different types of nanocellulose. The first one is a top-down process which is used to produce cellulose nanofibers (CNF) and cellulose nanocrystals (CNC) from plants. This process is applied to lower the size of the fibers down to nano scale [14–17]. The second route is a bottom-up process by which bacterial cellulose (BC) can be synthesized from cellulose-producing bacteria (such as the *Acetobacter xylinus* and the *Komagataeibacter xylinus* species) in the fermentation process of low molecular weight sugar [18].

Applications of CNF in cementitious composites have been extensively investigated in the past few years. High Young's modulus (65–110 GPa) [19], large aspect ratio (4–20 nm width, 500–2000 nm length) [20], and thermal stability [21] have enabled CNF to improve mechanical properties such as elastic modulus, flexural and compressive strengths of cementitious composites [22,23]. In addition to the mechanical performance enhancement, CNF has shown great potential for improving the durability performances of cement-based composites [24, 25]. Moreover, the addition of CNF in cement composites can increase

E-mail address: warda.ashraf@uta.edu (W. Ashraf).

^{*} Corresponding author.



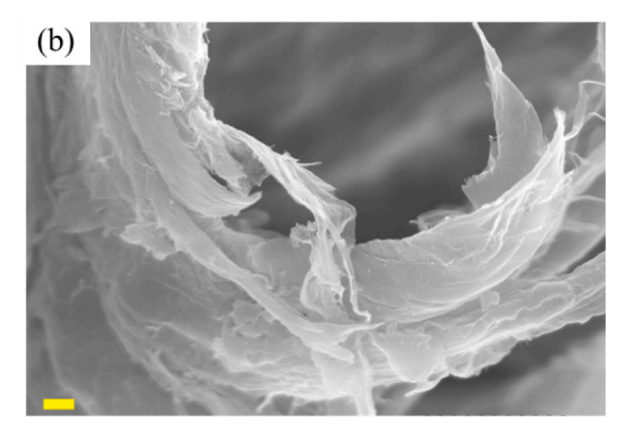


Fig. 1. Scanning electron microscopic (SEM) images of the cellulose nanomaterials (a) Bacterial cellulose (BC), (b) Cellulose nano fibers (CNF). The scale bar represents a distance of $2 \mu m$.

the degree of hydration, reduce the setting time and densify the microstructure [22,26–29].

Nanocellulose can also help reducing the formation of shrinkage cracks in concrete. Deleterious autogenous shrinkage cracks occur at very early ages before the cementitious composites gain sufficient strength. Among various strategies, 'internal curing' can be a potential solution to resist this problem by providing additional curing water through the inclusion of water-saturated porous materials in the hydrating cement paste [30,31]. It is widely accepted that adding cellulose fibers to cement-based systems helps control the properties of drying shrinkage cracking and plastic shrinkage [32-36]. Additionally, since cellulose fibers can be dispersed in hydrating cement paste and have the capacity to absorb and release water, they can be considered as potential internal curing agents. Previous studies [9,10,30,37] showed that, for mortar, a 1% and 2% addition of cellulose fibers by mass of cement led to a 13% and 32% reduction respectively in autogenous deformation at 7 days. Then, the addition of 0.06% and 0.09% CNF into the cement paste reduced the autogenous shrinkage up to 49% and 26% respectively.

Compared to CNF, the applications of BC in cementitious composites have not been well investigated yet. Nevertheless, the utilization of BC for environmental purposes is a quickly developing field of engineering [38]. BC is an organic compound with the same chemical formula, $(C_6H_{10}O_5)_n$ as CNF. Bacterial cellulose shows high levels of crystallinity (60%) and a higher degree of polymerization (16,000–20,000) and purity compared to the plant cellulose [39,40]. It also has a higher water absorption capacity and high tensile strength (200–300 MPa), as well [40,41]. In the past, BC was used for the surface treatment of fibers in the production of bagasse fiber–cement composites [42]. Furthermore, researches showed that nanocellulose materials were able to improve the healing capacity of cementitious composites [43].

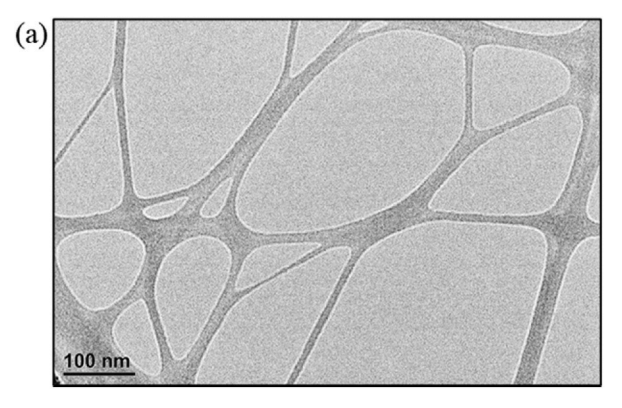
Based on the above-mentioned discussions, nanocellulose have

clearly emerged as a promising additive for improving the performance of cement-based composites. However, the differences between the roles of CNF and BC with respect to cement-based composites are not well understood yet. Therefore, the primary objective of this article is to highlight the differences in the effects of CNF and BC on the macro to nano structural aspects of cementitious composites. At the macroscale, the effects of nanocellulose on the strength and alkali-silica reaction of mortar samples were monitored. The microscale investigation comprised of monitoring the effects of nanocellulose on cement hydration, hydration products, microstructure, and microporosity. To understand the effects of nanocellulose at the nanoscale of cementitious materials, the nanomechanical properties and the nanoporosity of the cement paste samples were evaluated.

2. Materials and methods

2.1. Raw materials

The effects of nanocellulose on cement hydration and microstructure were monitored using paste samples. Ordinary portland cement (type I/II) and nanocellulose were used to prepare these samples. The ordinary portland cement (OPC) met the ASTM C150 [44] specification. Based on the X-ray fluorescence test, OPC contained 21.2% SiO₂, 65.3% CaO, 3.9% Al₂O₃, 3.1% Fe₂O₃. The bacterial cellulose (BC) and cellulose nanofibrils (CNF) were supplied by a commercial company, Cellulose Lab, located in Canada. The origin of the CNF was bleached sulfate hardwood pulp, and the BC was produced by *Acetobacter xylinum* bacteria. The raw nanocellulose samples were in slurry form and the composition was 1% weight solid in water. Fig. 1 represents the scanning electron microscopic (SEM) images of the raw BC and CNF. These fibers were appeared to form like thin films. The transmission electron



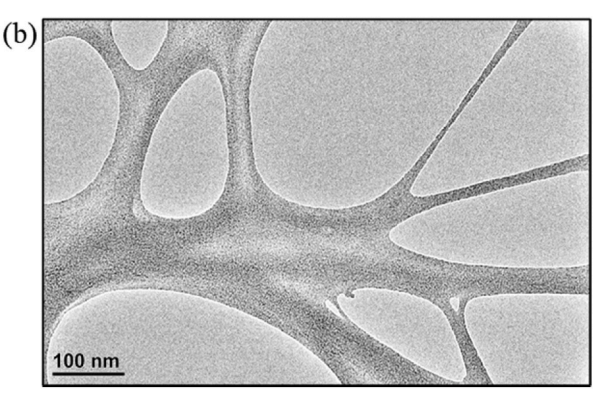


Fig. 2. Transmission electron microscopic (TEM) images of the cellulose nanomaterials (a) Bacterial cellulose (BC), (b) Cellulose nano fibers (CNF).

Table 1
Matrix of experiments with number of samples and sample type.

Tests	Dosages Testing age		Number of samples	Sample type	
Zeta potential measurement	Control	0 days	1	Raw diluted samples	
	0.3% CNF		1		
	0.3% BC		1		
Heat of hydration	Control	Up to 7 days	1	Cement paste ($w/c = 0.35$)	
	0.05% CNF		1		
	0.05% BC		1		
	0.1% CNF		1		
	0.1% BC		1		
	0.3% CNF		1		
	0.3% BC		1		
Thermogravimetric Analysis (TGA)	Control	7, 28, 56 & 90 days	4	Cement paste ($w/c = 0.35$)	
	0.05% CNF	•	4	•	
	0.05% BC		4		
	0.1% CNF		4		
	0.1% BC		4		
	0.3% CNF		4		
	0.3% BC		4		
Scanning Electron Microscopy (SEM)	Control	0 & 28 days	1	Cement paste ($w/c = 0.35$)	
17 ,	0.3% CNF	•	1	•	
	0.3% BC		1		
Mercury Intrusion Porosimetry (MIP)	Control	28 days	1	Cement paste ($w/c = 0.35$)	
,	0.3% CNF		1	, , , , , , , , , , , , , , , , , , ,	
	0.3% BC		1		
Dynamic Vapor Sorption (DVS)	Control	28 days	1	Cement paste ($w/c = 0.35$)	
-, - (,	0.3% CNF		1	, , , , , , , , , , , , , , , , , , ,	
	0.3% BC		1		
Nanoindentation	Control	28 days	1	Cement paste ($w/c = 0.35$)	
Tunomuchanon	0.3% CNF	20 00,0	1	coment paste (11, c c clob)	
	0.3% BC		1		
Compressive strength test	Control	7, 28, 56 & 90 days	12	Cement paste ($w/c = 0.35$)	
dompressive strength test	0.05% CNF	7, 20, 50 to 50 taly5	12	Gement paste (w/c = 0.55)	
	0.05% BC		12		
	0.1% CNF		12		
	0.1% BC		12		
	0.3% CNF		12		
	0.3% BC		12		
Flexural strength test	Control	7, 28, 56 & 90 days	12	Cement paste ($w/c = 0.35$)	
i icati di diciigiii test	0.05% CNF	7, 20, 30 & 30 days	12	Geniciti paste (w/c = 0.55)	
	0.05% BC		12		
	0.1% CNF		12		
	0.1% GNF 0.1% BC		12		
	0.1% BC 0.3% CNF		12		
	0.3% GNF		12		
Alkali Silica Reaction (ASR) test	Control	Up to 16 days	4	Mortar $(w/c = 0.50)$	
AIRAII SIIICA REACTIOII (ASR) test		op to 10 days		Mortar ($w/c = 0.50$)	
	0.05% CNF		4		
	0.05% BC				
	0.1% CNF		4		
	0.1% BC		4		
	0.3% CNF		4		
	0.3% BC		4		

microscopic (TEM) images (Fig. 2) also confirmed that the agglomerations of the nanofibers were apparent at the nanoscale too. Accordingly, it was difficult to measure the aspect ratio or fiber dimensions using SEM or TEM images. Based on the information provided by the supplier, the width and length of the cellulose nanofibrils were 20–60 nm and several micrometers, respectively. On the other hand, the width of the bacterial cellulose was 50–100 nm, and the length was around 30 μm .

Most of the studies on cementitious materials showed high improvements with nanocellulose doses lower than 1 wt%, and some of them have proved that the effects of nanocellulose can be reverted if they are overdosed [11,45–47]. Therefore, 0% (control), 0.05%, 0.1% and 0.3% dosages were chosen. The water to cement ratio for the cement paste was 0.35.

To monitor the effects of nanocellulose on alkali silica reactivity, the ASTM C1260 [48] test was performed. For this experiment, mortar samples were prepared with the sodium borosilicates as reactive aggregates maintaining w/c of 0.50 and cement to aggregate ratio of 2.25. The details of this test method are given in section 2.3.10.

2.2. Sample preparation

For the paste sample preparation, first, the nanocellulose material was added to the water in the mixer and mixed at a slow speed (140 \pm 5 r/min) for 60 s. Then, cement was added to the mixer and the speed was changed to medium (285 \pm 10 r/min) for 2 min.

For the mortar batches, first, the nanocellulose was mixed in the water at a slow speed (140 \pm 5 r/min). Next, the cement was added to the mixer and mixing was continued for 30 s. After that, the entire quantity of sodium borosilicate was added slowly over a 30 s period while mixing at slow speed (140 \pm 5 r/min). Next, the speed was changed to medium (285 \pm 10 r/min), and the mixing was continued for 30 s. Then, the mixer was stopped for 90 s and the materials on the side of the bowl were scrapped down into the mixing bowl. Lastly, the mixing was finished by continuing for another 60 s at medium speed (285 \pm 10 r/min). Table 1 represents the matrix of experiments with total number of samples and sample type.

2.3. Experimental methods

2.3.1. Zeta potential measurement

The zeta potential of the BC and CNF samples were measured using Malvern Zetasizer 3000. One gram of nanocellulose suspension was mixed with 80 g of pH 7 solution and allowed to homogenize for 2 min before measuring the zeta potential.

2.3.2. Heat of hydration

Paste samples were prepared by mixing cement with water and nanocellulose as per the ratios mentioned in section 2.1. After mixing, approximately 15 g of each paste sample was placed in a glass vial to monitor the heat of hydration. An isothermal calorimeter (TAM Air, TA instrument) was used to measure the heat release from the cement paste over 100 h at an ambient temperature of 25 °C. The effects of the nanocellulose on the cement hydration products were determined by performing thermogravimetric analysis (TGA).

2.3.3. Thermogravimetric analysis (TGA)

BC and CNF paste samples were used for thermogravimetric analysis (TGA). Isopropanol was used to stop the hydration of the cement paste samples after 7, 28, 56 and 90 days of sealed curing following the solvent exchange method. The cement paste samples were then dried in a desiccator for 24 h to avoid atmospheric carbonation. Finally, the dried paste samples were ground using mortar-and-pestle and the powder was used for TGA measurements. A commercially available instrument (TA instrument, TGA 550) was used for the TGA measurements. Approximately, 30-40 mg of powder sample was tested for each batch. The powdered sample was loaded into a platinum pan and kept under isothermal condition at room temperature for 5 min. The temperature of the TGA furnace chamber was then raised up to 980 °C at an increment rate of 15 °C per min. Nitrogen was used as the purging gas during the experiment to maintain an inert environment. From this test, the quantitative amounts of chemically-bound water in C-S-H and Ca(OH)2 in the hydrated cement paste were determined.

2.3.4. Scanning electron microscope (SEM) imaging

The microstructures of the 28-day cured cement pastes containing CNF and BC were evaluated using the Hitachi 3000 N SEM. The instrument was operated in high vacuum mode with a 30 kV accelerated voltage and a working distance of about 10 mm. The cement paste sample was coated with Platinum (Pt) before capturing the SEM images.

2.3.5. Transmission electron microscope (TEM) imaging

TEM images of the bacterial cellulose (BC) and cellulose nanofibrils (CNF) were obtained dispersing them into isopropanol solution. For well uniform dispersion, the solution was ultrasonicated for 10 min with Cole-Parmer 8890. To collect the TEM images, firstly, the sample was taken into lacey carbon 300 mesh, gold grid (Ted Pella Inc, USA) and then, Hitachi H-9500 was used at 300 kV. All the TEM images were taken maintaining the same magnification level.

2.3.6. Mercury intrusion porosimetry (MIP)

Mercury intrusion porosimetry (MIP) is one of the main methods for investigating the mesoporous structure (pore radius between 2 and 50 nm) and the macro-porous nature (apertures greater than 50 nm) of cementitious materials. Its effectiveness is based on the principle that to fill a non-wetting fluid into a pore of diameter d, a pressure P inversely proportional to this diameter must be applied. This pressure is given by the Washburn equation below [49].

$$P = \frac{-4 \cdot \gamma \cdot \cos \theta}{d}$$

Where, P = Pore pressure, d = Pore diameter.

The surface tension of the mercury (γ) is well established and

generally researchers use $\gamma=0.485$ N/m at 25 °C [50]. The contact angle between mercury and cement paste θ is more difficult to determine, but after many investigations, researchers have agreed that $\theta=140^\circ$ [51].The contact angle can vary due to several factors like the chemical composition of the sample, the contamination of the surface, etc. [52,53].

For this research, the MIP test was performed on control batch and cement paste samples containing 0.3% nanocellulose dosages after 28 days of curing. The sample size was around $15\times15\times15$ mm. The surface tension γ of mercury is 0.485 N/m, and the average contact angle θ between mercury and the pore wall is 130° . MIP tests were conducted on an AutoPore IV 9500 V2.03.01, from Micrometrics Instrument Corporation, under a maximum pressure of 413 MPa to reach pores with a diameter of 3.02 nm.

2.3.7. Dynamic vapor sorption (DVS)

Commercially available DVS equipment (Q 5000, TA instruments) was used to obtain the sorption isotherms. The sample was first equilibrated at 97.5% RH for 5760 s. After this point, the RH was gradually reduced (with 5–10% RH steps) to obtain the desorption isotherm. After reaching 0%, the RH was gradually increased (with 5–10% RH steps) up to 97.5% to obtain adsorption isotherms. A constant temperature was maintained (23 $^{\circ}\text{C}$) during this experiment. The DVS measurements were obtained from control batch and cement paste samples containing 0.3% nanocellulose dosages after 28 days of curing. A thin slice of around 1 mm thickness and 3–4 mm width was cut from the cement paste cubes using a water-cooled saw. The sliced samples were then soaked in deionized water for around 24 h to ensure full saturation of the pores before the measurements.

2.3.8. Nanoindentation test

To prepare the sample for nanoindentation, first, a half disc of the paste sample, approximately 20 mm in diameter and 10 mm thick, was cut using a slow-cutting laboratory saw machine cooled with mineral oil. Detailed sample preparations steps, test procedure and calculations regarding this can be found elsewhere [54].

For grid nanoindentation, cement paste samples containing 0.3% BC and CNF were chosen with the control batch samples after 28 days of sealed curing. The load function had three segments: (i) loading from zero to maximum load in the span of 5 s, (ii) holding at the maximum load for 5 s, (iii) unloading from maximum to zero load within 5 s. Selection of the appropriate load function is crucial for obtaining reliable nanoindentation data. This is because, on the one hand, the indentation depth should be large enough with sufficient accuracy as these are based on contact micromechanics. On the other hand, the depth of the indentations should also be small enough to determine the mechanical properties of the individual microscopic phases (i.e. indentation depth « characteristic size of each microscopic phases) [54]. Considering both criteria, the load function with a maximum load of 3000 µN was selected for the SNI technique during this study. The average indentation depth for this load function was around 200–350 nm for a 30 μ m \times 30 μ m area containing all microscopic phases.

Nanoindentation tests were performed using a Hysitron Triboindenter UB1 system (Hysitron Inc. Minneapolis, USA) fitted with a Berkovich diamond indenter probe. The tip area function was calibrated by performing several indents with various contact depths on a standard fused quartz sample.

Due to the heterogeneous nature of the microstructures containing multiple phases, a large number (\sim 225) of indentations needed to be performed on each individual specimen. To aid in the interpretation of the data, the resulting experimental values of the elastic modulus are presented in the form of frequency distribution plots. These plots are, in turn, analyzed using the statistical deconvolution method [55,56] to estimate the intrinsic modulus of the individual phases. These include the mean elastic modulus of each phase and their volume fractions, both of which were estimated based on the best fit of the experimental data

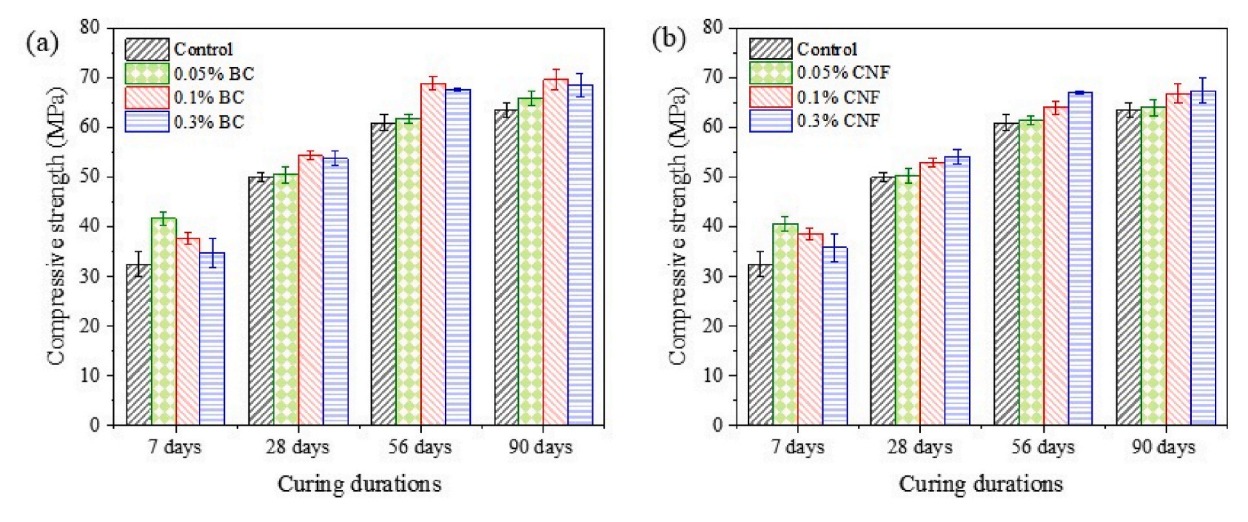


Fig. 3. Compressive strength of different (a) bacterial cellulose dosages and (b) cellulose nanofibrils dosages.

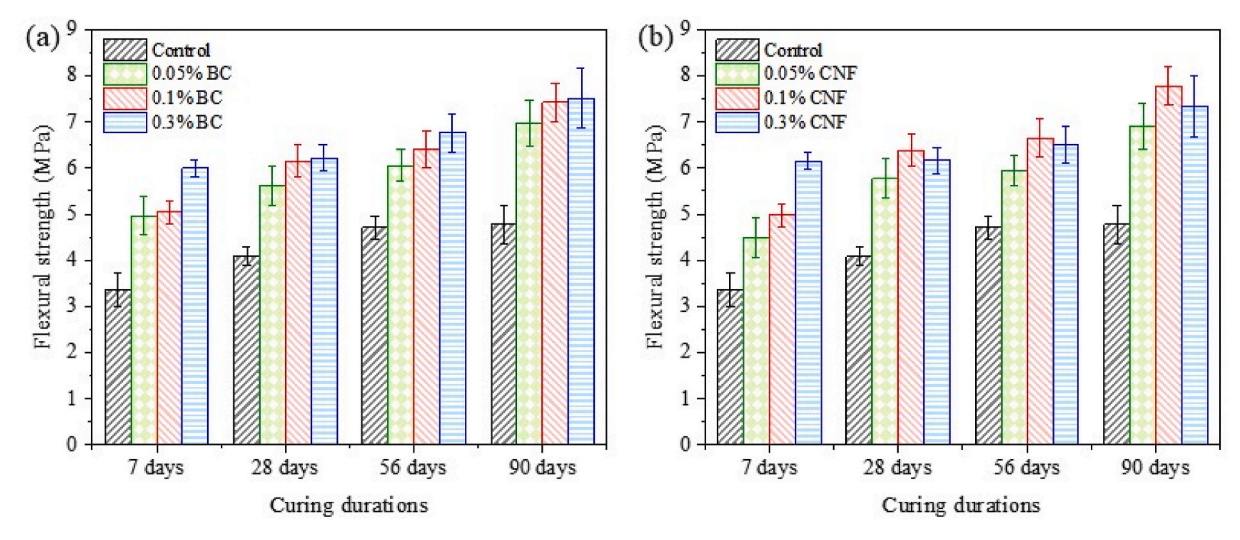


Fig. 4. Flexural strength of containing different (a) bacterial cellulose dosages and (b) cellulose nanofibrils dosages.

with a limited number of Gaussian distribution functions.

2.3.9. Compressive and flexural strength tests

A total of 7 batches of cement pastes with w/c of 0.35, and with different BC and CNF contents were prepared for a compressive strength test. A sealed curing condition was adopted by covering the fresh paste samples with a plastic sheet and keeping them at 23 °C for 24 \pm 1 h. After this period, the samples were demolded and stored in sealed plastic bags at 23 °C temperature until the age of testing. Compressive strengths were measured for the paste cube (50 mm sides) samples as per ASTM C109 [57] using a loading rate of 900–1800 N/s. Compressive strengths were determined after 7, 28, 56, and 90 days of sealed curing.

The flexural strength was determined by performing the three-points bending test of beam samples with dimensions of 40 mm \times 40 mm \times 160 mm. The paste samples were tested after 7, 28, 56 and 90 days of sealed curing.

2.3.10. Alkali silica reaction (ASR) test

A recycled, crushed type 33 alkali-borosilicate glass (NBS, Vitro Minerals) was used as a model reactive siliceous aggregate. The ASTM C1260 [48] standard test method was followed to conduct this experiment. As per the specification, the dimension of the mortar beams were 25 mm \times 25 mm \times 285 mm, having a 250 mm gauge length as per the standard ASTM C490 [58]. After the beam samples had been cast in the

molds, they were kept in a moist cabinet for 24 h. Next, the specimens were removed and placed in a storage container submerged under water at 23 $^{\circ}\text{C}$ for a period of 24 h. Then, upon drying the samples, zero readings were taken, and after that the samples were put under a 1 N NaOH solution at 80 $^{\circ}\text{C}$. The length changes were noted down every 24 h for 16 days.

3. Results and discussion

3.1. Surface potentials of bacterial cellulose (BC) and cellulose nanofibrils (CNF)

The absolute values of the zeta potential measurement of the BC and CNF slurries were found to be 0.19 mV and 30 mV, respectively. The higher surface charge allowed higher dispersion stability of the CNF in water suspension [46,59]. Moreover, the higher negative values of the zeta potential indicated that the strong electrostatic repulsion between particles would prevent their aggregation and thereby stabilize the nanoparticulate dispersion [60]. The CNF was negatively charged due to free hydroxyl groups (OH) [61]. Based on this finding, it is apparent that BC will have a higher tendency of agglomeration compared to that of CNF.

Table 2Statistical (*t*-test) analysis results (*p*-values) of compressive and flexural strength of BC batches.

BC dosage	Compressive strength Curing age				Flexural strength Curing age			
	0%	_	_	_	_	_	_	_
0.05%	0.01	0.33	0.28	0.09	0.00	0.02	0.04	0.02
0.1%	0.02	0.02	0.00	0.00	0.00	0.00	0.06	0.04
0.3%	0.38	0.08	0.00	0.00	0.00	0.03	0.05	0.00

^{*}Note: Bold fonts (*p*-values>0.05) represent that the data are not statistically significant.

Table 3Statistical (*t*-test) analysis results (*p*-values) of compressive and flexural strength of CNF batches.

CNF dosage	Compressive strength Curing age				Flexural strength Curing age			
	0%	-	_	_	_	_	-	_
0.05%	0.02	0.39	0.33	0.34	0.01	0.01	0.07	0.13
0.1%	0.03	0.01	0.03	0.04	0.01	0.00	0.04	0.04
0.3%	0.21	0.01	0.01	0.04	0.00	0.02	0.01	0.01

^{*}Note: Bold fonts (*p*-values>0.05) represent that the data are not statistically significant.

3.2. Macroscale effects of CNF and BC

3.2.1. Effects of nanocellulose on compressive and flexural strengths

Fig. 3 shows the effects of nanocellulose on the compressive strengths of the cement paste after different curing durations. Both types of nanocellulose increased the compressive strength of the cement paste by nearly 30% after 7 days of curing at 0.05% dosage. Such superior strength at the early age due to the addition of CNF or BC was attributed to the hydration acceleration effects of these nanomaterials (further discussed in 'heat of hydration' section). It was observed that the addition of 0.1% BC increased the compressive strength by around 10% after 90 days of curing. On the other hand, addition of 0.3% CNF showed the highest compressive strength, which was 10% higher than the control batch. Nanocellulose can act as an 'internal curing' agent in cement paste samples [9]. Such internal curing might have resulted in a uniform— higher degree of hydration and denser microstructure in the nanocellulose-containing batches compared to the control batch, and

therefore, resulted in a higher compressive strength.

Fig. 4 shows the flexural strengths of the cement paste samples with and without the nanocellulose additions. The beneficial effects of nanocellulose on the flexural strengths of cement paste were significantly more pronounced compared to those observed in the case of compressive strength. After 7 days of curing, the flexural strength of the cement paste containing 0.3% CNF or 0.3% BC was increased by nearly 100%. In the case of BC, a higher dosage resulted in higher flexural strengths. On the other hand, for CNF, 0.1% was observed to be the optimum dosage to improve the flexural strength. Addition of 0.3% BC increased the flexural strength by 57%, whereas 0.1% CNF dosages increased the flexural strength by 63% compared to the control batch after 90 days of curing. Therefore, in the case of flexural strength enhancement, CNF performed slightly better than the BC. Such beneficial effects of CNF and BC confirms that both of these nanomaterials can act as nano-reinforcement to bridge the microcracks in cement paste [46].

The statistical significance of the effects of nanocellulose on the compressive and flexural strengths of mortar samples were evaluated using the t-test. In this case, the level of statistical significance was expressed as the p-value. The compressive strength and flexural strength results were compared with respect to the 0% nanocellulose dosage. The test was conducted at a confidence level of 95%. Statistical p-values less than 0.05 indicated a statistically significant difference between the two

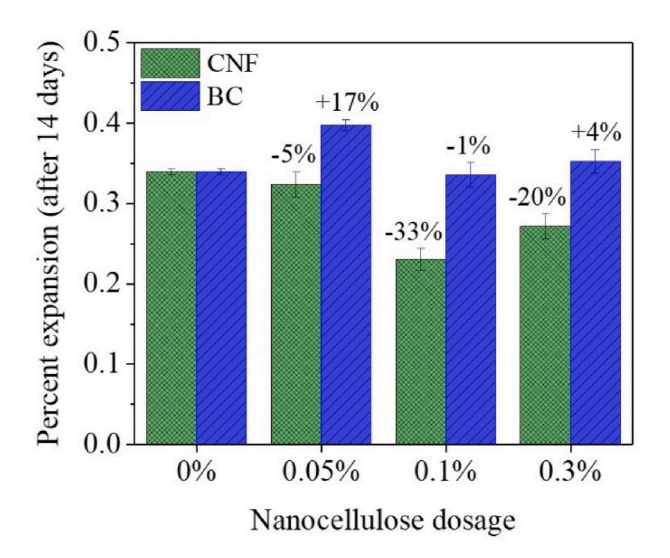
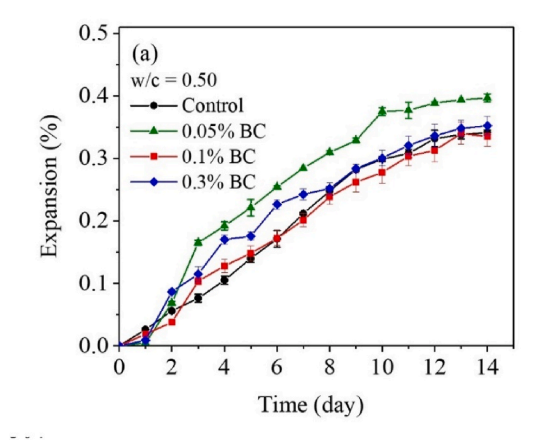


Fig. 6. Comparison of percent expansion due to alkali silica reaction after adding different dosages of nanocellulose (after 14 days).



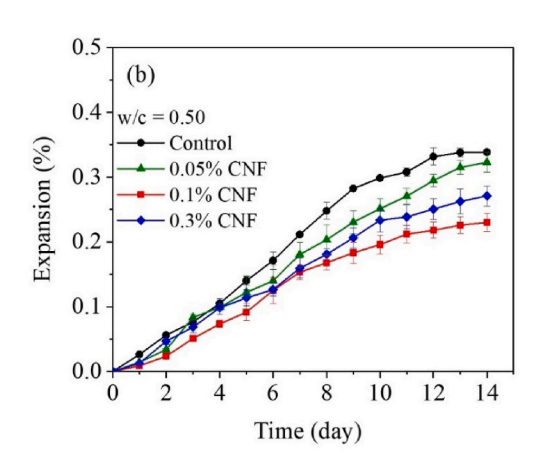


Fig. 5. Percent expansion due to alkali silica reaction (a) BC batches, (b) CNF batches.

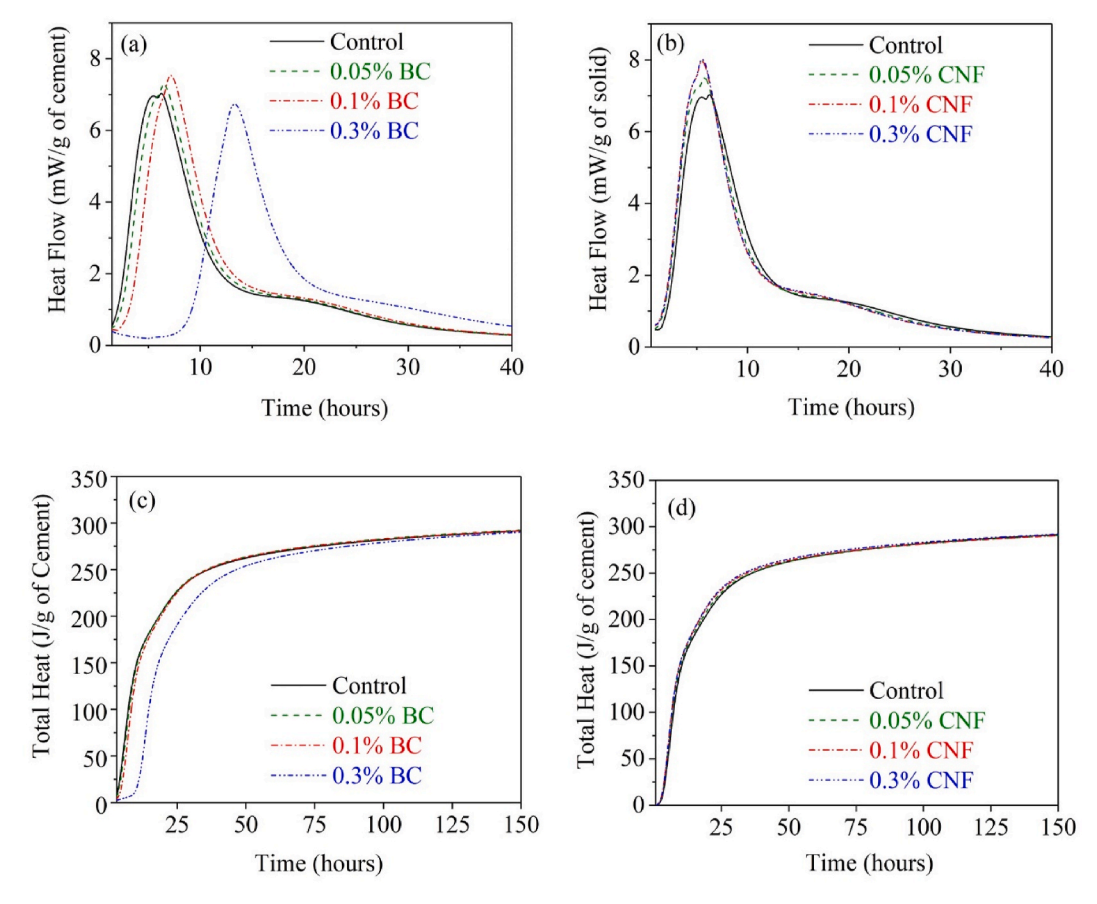


Fig. 7. (a) Heat flow per g of cement (BC); (b) Heat flow per g of cement (CNF); (c) Total heat per g of cement (BC); (d) Total heat per g of cement (CNF).

groups of samples and vice versa.

The results of the statistical analyses for the BC and CNF containing samples are given in Table 2 and Table 3, respectively. As observed from these tables, at a low dosage (i.e., 0.05%), nanocellulose does not significantly improve the compressive strength of cement paste. Nevertheless, at higher dosages (that is 0.1% and 0.3%), both types of nanocellulose significantly enhanced the compressive strengths of the cement paste. On the other hand, nanocellulose can significantly enhance the flexural strength even at a low dosage of 0.05%.

3.2.2. Nanocellulose for ASR suppression

In addition to mechanical performance, application of nanocellulose to improve durability performances has also gained tremendous interest [24,25]. Because of nanocellulose's affinity for alkali ions, we investigated the potential role of these materials to mitigate the alkali-silica reaction (ASR). The ASR occurs between the alkalis present in the cement pore solution and the reactive aggregate. This reaction forms expansive gels that results in cracking and, eventually, leads to the degradation of the mechanical properties of concrete [62–64]. By reducing the availability of alkali ions, nanocellulose could reduce the detrimental effects of ASR.

Fig. 5 shows the trend of percent expansion after addition of different nanocellulose dosages. As expected, due to the usage of reactive borosilicate glass aggregates, the control mortar batch showed a high expansion level. However, after the addition of BC, the expansion due to ASR remained the same. There was even a slight increase in expansion with the addition of 0.05% BC. Such increased expansion can be attributed to the hygroscopic properties of BC. On the other hand, the addition of CNF helped to reduce the expansion caused by ASR. It was observed that the addition of 0.1% CNF was able to lower the expansion of the mortar bar by 33% after 14 days of measurement. The other

dosages of CNF, 0.05% and 0.3% also reduced the ASR reaction by 5% and 20%, respectively. The comparison of percent expansion due to different nanocellulose dosages is shown in Fig. 6. Important to note, based on the zeta potential measurements, CNF had a higher negative surface charge ($-30\,\text{mV}$) compared to that of BC ($+0.19\,\text{mV}$). Therefore, even though CNF and BC have same molecular structure, the number of the negatively charged hydroxyl (OH $^-$) and carboxyl (COOH $^-$) surface groups in CNF is expected to be higher compared to that of BC. These negatively charged surface groups of CNF can bind alkali ions (K $^+$ and Na $^+$). Due to the reduced availability of alkali ions, the extent of ASR gel formation may have been reduced, and therefore, expansion was also lowered by the addition of CNF as observed from the length change measurements.

3.3. Microscale effects of CNF and BC

3.3.1. Effects of nanocellulose materials on cement hydration

Fig. 7 (a) and (b) shows the rate of heat evolution of cement pastes with different nanocellulose dosages up to first 40 h of hydration. The effects of BC and CNF were evaluated by comparing the primary exothermic heat flow peak and total heat release up to 150 h of hydration (Fig. 7 (c) and (d)). Initially, it was observed that the heat flow was accelerated due to the addition of CNF, whereas BC delayed the early age hydration. The accelerating effect was attributed to the additional surface area provided by the CNF. This additional surface area worked as the nucleation sites for CSH which also increased the nucleation rate of CSH [65–67]. The increased rate of CSH nucleation enhanced the cement hydration during the acceleration period [68,69]. Similar acceleration of cement hydration due to the addition of CNF has been observed previously [46]. Contradictorily, the addition of BC was found to delay the early-stage cement hydration reaction. Specifically, the

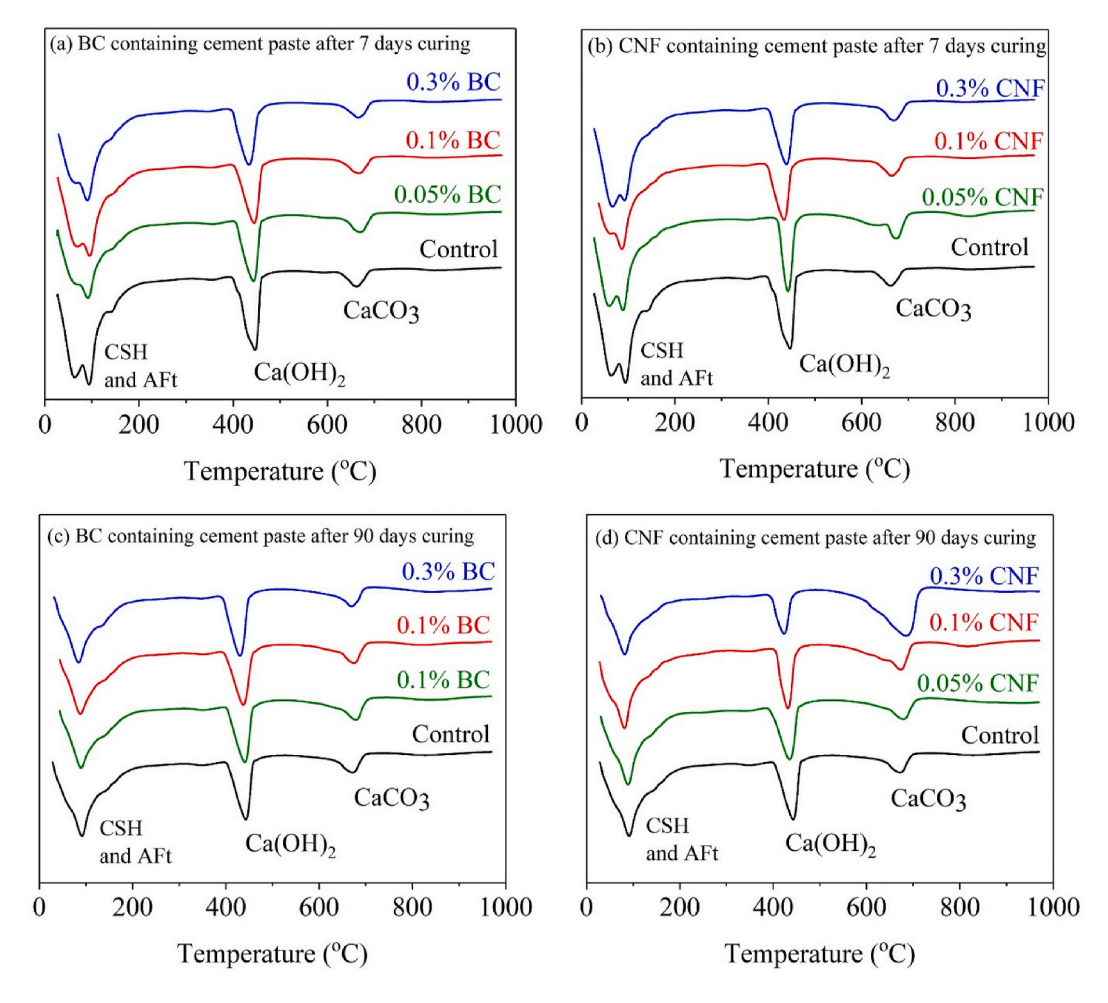


Fig. 8. Typical TGA-DTG plot of BC and CNF after 7 and 90 days of sealed curing.

addition of 0.3% BC delayed the acceleration period by around 7 h. Such a substantial delay can be attributed to the agglomeration of BC, as indicated by the zeta potential measurements. Nevertheless, the total heat release after 150 h of hydration was same for cement samples with and without BC and CNF. Therefore, even though the additions of CNF and BC affected the early-stage hydration, the degree of hydration was the same after 7 days of curing.

3.3.2. Effects of nanocellulose materials on cement hydration products

The composition of the hydrated cement paste was evaluated by TGA and derivative of thermogravimetric (DTG) graphs. Fig. 8 represents the typical TGA and DTG curve after 7 and 90 days of sealed curing. The DTG can be used to locate the temperature ranges corresponding to thermal decompositions of different hydrated phases present in cement paste [70,71]. The TGA data was further analyzed to quantify the amounts of Ca(OH) $_2$ and chemically bound water present in CSH. The amounts of Ca(OH) $_2$ were determined by integrating the DTG peak in the temperature range of 400–500 °C [71]. The chemically bound water content of CSH was determined by subtracting the weight loss corresponding to Ca(OH) $_2$ decomposition from total weight loss in the temperature range of 150 °C and 600 °C.

Fig. 9 presents the CH and CSH bound water contents in cement paste with different dosages of BC and CNF. As observed from Fig. 9 (a) and (b), after 7, 28, 56 and 90 days both BC and CNF resulted in lower CH contents compared to those of the control batch. On the other hand, the chemically bound water present in CSH was actually increased due to the addition of cellulose nano materials. The increase in chemically bound water content indicated that the addition of BC or CNF enhanced

the degree of hydration after a long curing duration. Such enhanced hydration due to the addition of nanocellulose was previously reported by Cao et al. [72]. The presence of carboxyl and hydroxyl groups on the surface of cellulose made it active in hydrated cement paste, and pore water was likely to be trapped on the surface, promoting hydration [25]. However, during our previous studies [46], such an increased degree of hydration was not observed. Therefore, we conclude that the role of nanocellulose on the degree of hydration after long-term curing depends on the source of the nanocellulose. All of the dosages of BC and CNF resulted in a lower amount of CH compared to the control batch. This observation is similar as before [73], and can be attributed to the Ca²⁺ binding by the carboxyl surface sites of nanocellulose.

3.3.3. Microstructure of cement paste with and without BC and CNF

Fig. 10 (a) shows the microstructure of the control batch without the inclusion of cellulose. Fig. 10 (b) and (c) show the SEM images of cement paste containing BC and CNF, respectively. Cellulose fibers are marked with yellow dotted lines in the images. Microstructure analysis was performed on the batches with 0.3% dosages of cellulose since cellulose was easily visible in this case. The formations of ettringite and CSH gel are clearly visible in the control batch (Fig. 10 (a)). As observed from Fig. 10 (b) and (c), the fibers protruded from the fractured cement paste surface. Such pull-out failure type indicates that these fibers were bridging the cracks of the cement paste. The visible fiber diameter in the cement paste batches containing BC was around 60 nm, while the visible fiber diameter in CNF was around 30 nm. The distribution of fibers appeared to be uniform throughout the matrix.

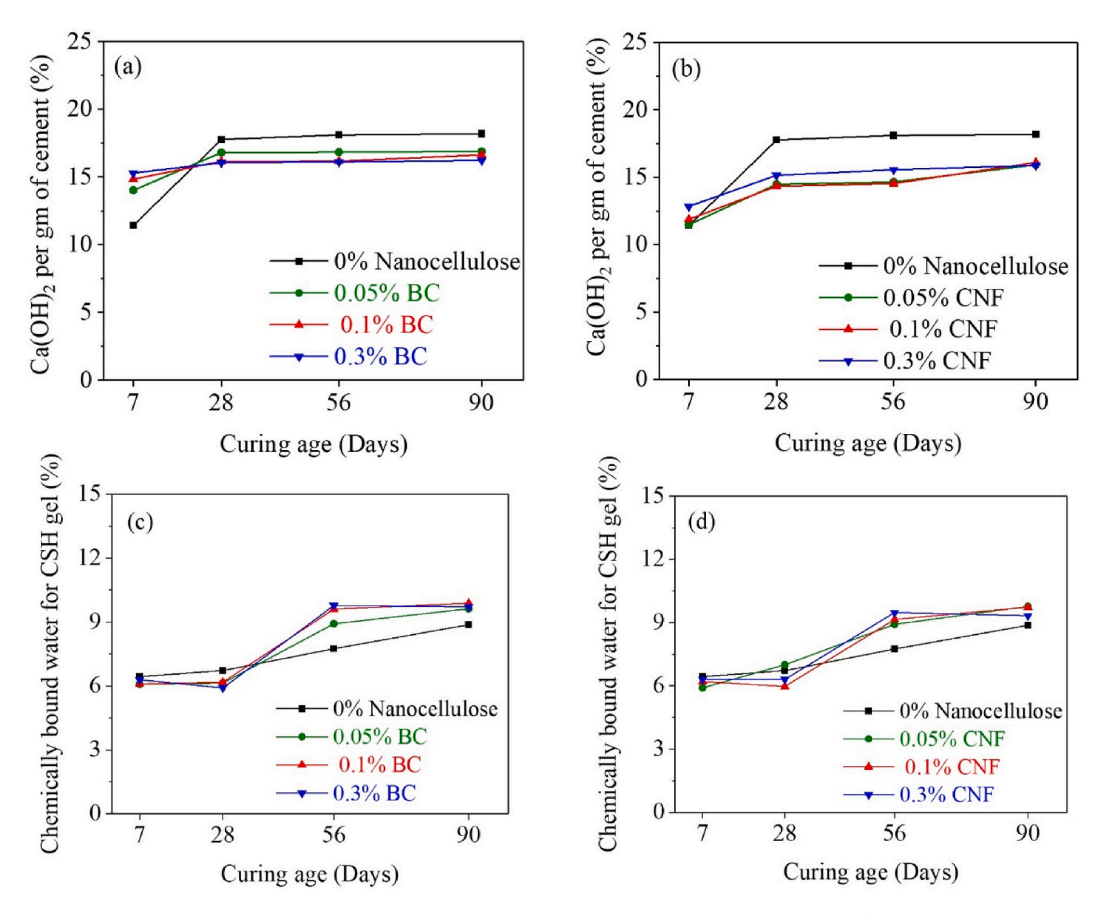


Fig. 9. (a) CH contents due to different dosages of BC, (b) CH contents due to different dosages of CNF, (c) Chemically bound water for CSH gel due to different dosages of BC, (d) Chemically bound water for CSH gel due to different dosages of CNF.

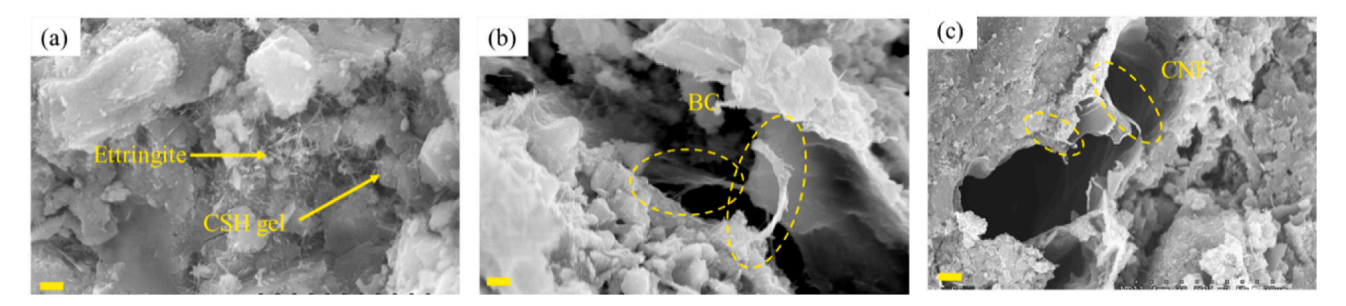


Fig. 10. SEM images showing the microstructure of 28 days cured cement paste containing (a) 0% CNF/BC, (b) 0.3% Bacterial cellulose (BC), (c) 0.3% Cellulose nanofibrils (CNF). The scale bar represents $2 \mu m$.

3.3.4. Pore size comparison by mercury intrusion porosimetry (MIP)

Fig. 11 shows MIP results conducted on control and 0.3% nanocellulose batches after 28 days of curing. Fig. 11 (a) indicates that the samples containing BC had lower porosity compared to the control and CNF containing batches. However, the addition of CNF was found to increase the total porosity compared to that of the control batch. The incremental intrusion curves shown in Fig. 11 (b) provide extended information on pore structure. As observed from this figure, the additions of both BC and CNF reduced the amounts of larger porosity and increased the amounts of smaller pores in the hydrated cement paste. Thus, both types of nanocellulose caused pore refinement of the hydrated cement paste matrix. CNF noticeably reduced the critical pore diameter of the cement paste compared to those observed in the case of the control batch. Such pore refinement effect due to the addition of nanocellulose was attributed to the higher degree of hydration (i.e., higher amounts of chemically bound water) as observed from the TGA

results. It was expected that both CNF and BC increased the amounts of CSH present in the hydrated matrix.

3.4. Nanoscale effects of BC and CNF

3.4.1. Nano-structural properties

Vapor sorption analysis is generally considered as the preferred technique for characterizing the CSH present in the cementitious matrix compared to MIP or nitrogen sorption, because: (i) water has the smallest molecular size compared to nitrogen or mercury, and thus, can access smaller pores; and (ii) as reported by Odler [74], differences in the employed temperature for water and nitrogen adsorption, causes water to pass over the energy barrier required for diffusion about 50 times more rapidly than nitrogen (nitrogen would take several years to equilibrate). Thus, the nitrogen sorption technique in general underestimates the surface area of cementitious matrixes in comparison to

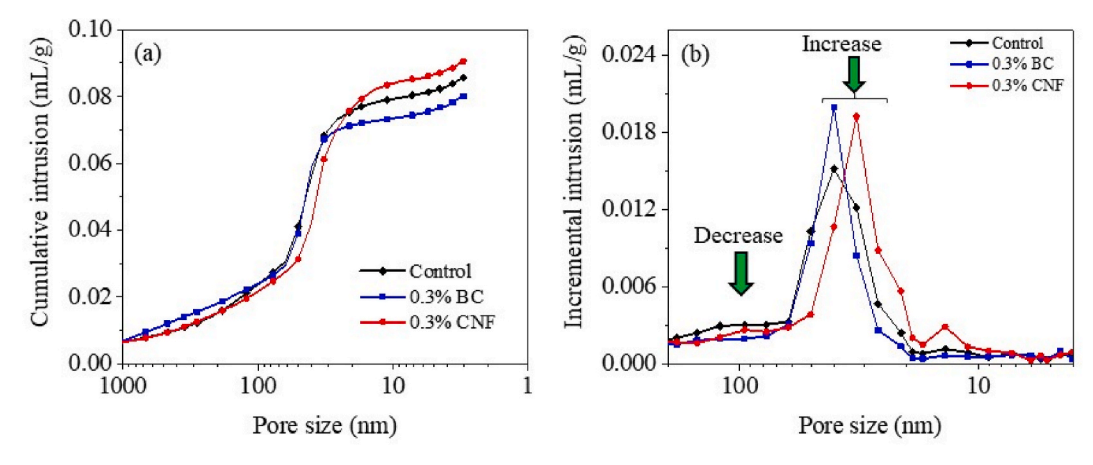


Fig. 11. (a) Cumulative intrusion vs pore size due to 0.3% nanocellulose dosage, (b) Incremental intrusion vs pore size due to 0.3% nanocellulose dosage.

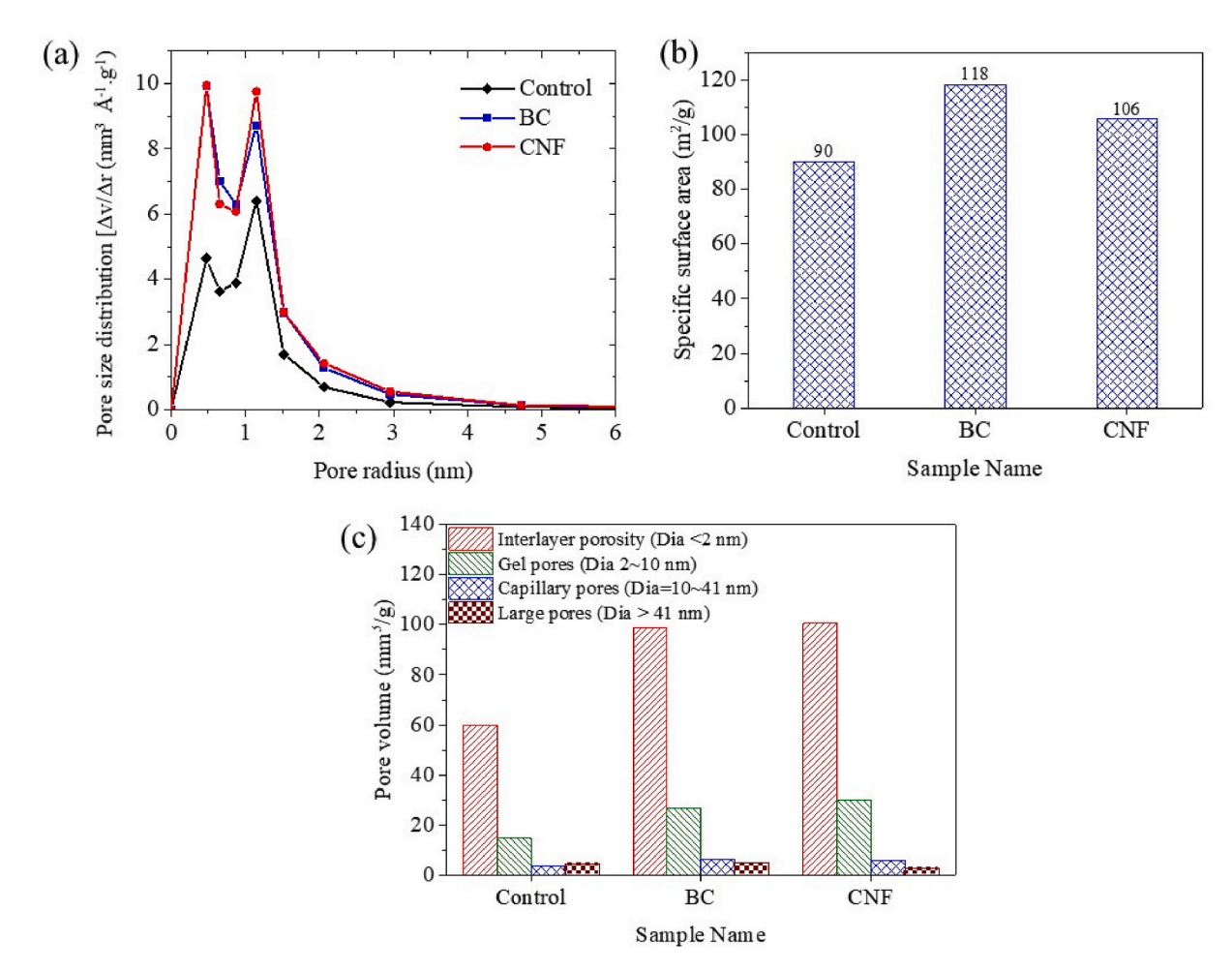


Fig. 12. (a) Pore size distribution, (b) specific surface area, and (c) volume of different pore categories for paste samples with and without cellulose nanofibers.

that of water sorption. Fig. 12 shows the pore size distributions in the cement paste samples with and without nanocellulose. From these graphs, two major peaks in pore sizes were observed for all of the cement paste matrixes at around 11.4 Å and 5 Å radius. The peak at 11.4 Å represents the interlayer porosity of CSH. As observed from Fig. 12 (a), there is no change in peak location; the intensity of this peak increased due to the addition of nanocellulose. This observation indicates that the addition of nanocellulose did not alter the structure/polymerization of CSH, but instead a higher amount of CSH was formed. This was also evidenced by the increase in specific surface area due to the addition of

nanocellulose [Fig. 12 (b)]. Following the convention similar to that used when describing the hydrated cement system [75], the distribution of different categories of pores in cement paste samples with and without nanocellulose are given in Fig. 12 (c). It can be observed that the additions of either BC or CNF significantly increased (more than 66%) both interlayer and gel porosity present in the cement paste. Therefore, the addition of nanocellulose essentially modified the nanostructure of the cement paste by forming additional CSH, and therefore densifying the matrixes. The addition of CNF resulted in a slightly higher amounts of interlayer and gel porosities compared to those of the BC containing

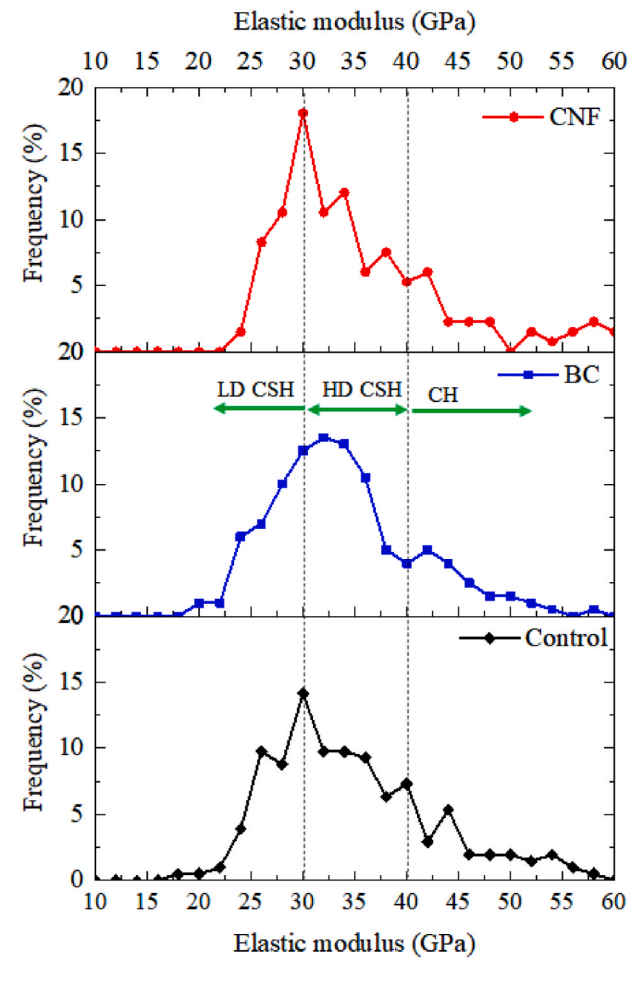


Fig. 13. Percent frequency vs elastic modulus of (a) control, (b) 0.3% BC and (c) 0.3% CNF after 28 days of sealed curing.

Table 4Relative proportions of cement hydration products as obtained from statistical nanoindentations.

Phase	Properties	Control	0.3% BC	0.3% CNF
LD CSH	Modulus (GPa)	27.4	25.9	28.3
	Standard deviation (GPa)	3.2	2.9	2.2
	Relative volume fraction	38.5	28.3	34.4
HD CSH	Modulus (GPa)	33.9	31.9	33.4
	Standard deviation (GPa)	3.7	2.8	5.02
	Relative volume fraction	24.2	42.4	50.9
CH	Modulus (GPa)	39.4	40.3	42.9
	Standard deviation (GPa)	7.7	5.7	5.6
	Relative volume fraction	37.3	29.3	14.7

samples.

3.4.2. Nanomechanical properties

Each sample was subjected to grid indentations over two different 60 $\mu m \times 60~\mu m$ areas, resulting in a total of 225 indentations. For all of these indentations, the values of the elastic modulus (E) and the hardness (H) values were calculated using equations given elsewhere [54]. The frequency distribution of the elastic modulus of the control, 0.3% BC, and 0.3% CNF batches are given in Fig. 13. Based on the literature data [76–78], approximate ranges for Low-density (LD) CSH, High-density (HD) CSH, and portlandite (CH) were marked in this figure. As observed from this figure, due to the addition of nanocellulose, the frequency was increased at around 35 GPa modulus. The

modulus frequency increase at around 35 GPa can be attributed to the increased amount of HD CSH. On the other hand, the frequency around 25 GPa, which represents LD CSH, was decreased due to the addition of nanocellulose. Such effect was more pronounced in the case of BC compared to that of the CNF.

To obtain a quantitative comparison, the cumulative frequency distributions functions (CDF) of the elastic modulus (E) were then statistically deconvoluted assuming normal frequency distribution function of elastic modulus values for all the individual microscopic phases. Details of the CDF deconvolution methods and the necessary explanations for this statistical process for determining the intrinsic elastic modulus of individual microstructural phases can be found elsewhere [55,56]. The deconvolution process yields the probability distribution function (PDF) of the elastic modulus (i.e., the mean and the corresponding standard deviation) for all of the microstructural phases. However, in this work, the deconvolution process was performed for the elastic modulus range of 0–60 GPa only to primarily focus on the cement hydration products. Table 4 represents the mean modulus, standard deviation, and volume fractions of LD CSH, HD CSH, and CH present in the cement paste with and without nanocellulose. The statistical deconvolution results confirm that the relative fraction of the LD CSH was decreased for the cement paste samples containing nanocellulose. Specifically, the relative volume fractions of LD CSH in the control, 0.3% BC, and 0.3% CNF containing batches were found to be 38.5%, 28.3%, and 34.4%. The relative amounts of the HD CSH were higher in the cellulose containing batches compared to that of the control batch. Cement paste containing 0.3% CNF was found to have the highest amount of HD CSH. This finding corroborated the observation from the MIP and vapor sorption pore analysis results, which showed that the CNF containing batch had higher amounts of smaller pores. Therefore, the addition of either type of nanocellulose made the cement paste matrix denser.

4. Conclusions

This article presented a comprehensive investigation on the effects of CNF and BC on the nano to macroscale properties of cement-based materials. The followings are the concluding remarks from this study:

- Nanocellulose significantly improved the compressive and flexural strengths of cement paste in the early stage (e.g., after 7 days of curing). At this curing duration, the compressive and flexural strengths due to the addition of nanocellulose were increased by nearly 30% and 100%, respectively.
- 2. After 90 days of curing, both types of nanocellulose increased the compressive and flexural strength of the mortar samples up to 10% and 60%, respectively. The suitable dosage of nanocellulose was found at 0.1% by weight of cement. A higher dosage (i.e., 0.3%) showed a decrease in compressive strength for BC and decrease in flexural strength for CNF.
- 3. The addition of 0.1% CNF was able to reduce the mortar bar expansion due to the ASR by 33%. Usage of BC did not show any significant effect on the ASR of the mortar bars.
- 4. BC was found to delay the early stage (less than 40 h) cement hydration, whereas CNF slightly accelerated the cement hydration.
- 5. After long-term curing (up to 90 days), cement paste samples containing either BC or CNF were found to contain lesser amounts of portlandite and higher amounts of CSH compared to that of the control batch. Accordingly, it was postulated that the addition of these nanomaterials improved the degree of cement hydration and entrapped calcium ions.
- 6. Based on the MIP results, the addition of BC reduced the total porosity of the cement paste. On the other hand, the addition of CNF reduced the size of critical porosity. Such effects on the porosity of the cement paste were attributed to the increased cement hydration after the addition of the nanocellulose.

7. Additions of nanocellulose were found to increase the amounts of HD CSH in the cement paste compared to the control batch. The amount of HD CSH was higher in the CNF containing batch compared to that of the BC containing samples.

Since addition of lower dosages of nanocellulose improved the flexural strength by up to 60%, it would help to reduce crack formation in real world structures like bridge deck, pavements, etc. Accordingly, by providing high flexural strength along with reduced autogenous shrinkage and expansion due to alkali silica reaction, nanocellulose can help concrete structures become more durable.

Based on the presented comparative investigation for the selected dosages of nanocellulose, CNF offers superior enhancement in ASR resistance, cement hydration rate, pore structure, and HD CSH formation in the cementitious system compared to BC.

Credit author statement

Muhammad Intesarul Haque: Data curation, Formal analysis, Investigation, Writing – original draft. Warda Ashraf: Conceptualization, Formal analysis, Investigation, Funding acquisition, Supervision, Writing - review & editing. Rakibul I. Khan: Data curation, Investigation. Surendra Shah: Supervision, Writing - review & editing.

Declaration of competing interest

The authors declare that no conflict of interest is involved in this paper and the authors are responsible for the content and writing.

Acknowledgement

This work was conducted with partial funding support from the US National Science Foundation (NSF # ECI - 2028462) and the P3Nano - U. S. Endowment for Forestry and Communities (#21-00184) for Dr. Warda Ashraf at the University of Texas at Arlington. All opinions, findings, and conclusions or recommendations expressed in this material are those of the authors and do not necessarily reflect the views of the sponsoring agencies.

References

- [1] R.J. Moon, G.T. Schueneman, J. Simonsen, Overview of cellulose nanomaterials, their capabilities and applications, J. Occup. Med. 68 (2016) 9.
- [2] O. Onuaguluchi, N. Banthia, Plant-based natural fibre reinforced cement composites: a review, Cement Concr. Compos. 68 (2016).
- [3] M.R. Hossen, N. Dadoo, D.G. Holomakoff, A. Co, W.M. Gramlich, M.D. Mason, Wet stable and mechanically robust cellulose nanofibrils (CNF) based hydrogel, Polymer 151 (2018).
- [4] C. Son, S. Chung, J. Lee, S. Kim, Isolation and cultivation characteristics of Acetobacter xylinum KJ-1 producing bacterial cellulose in shaking cultures, J. Microbiol. Biotechnol. 12 (5) (2002).
- [5] D. Mazlan, M.F. Md Din, C. Tokoro, I.S. Ibrahim, Cellulose nanocrystals addition effects on cement mortar matrix properties, Int. J. Adv. Mech. Civ. Eng. 3 (1) (2016).
- [6] S.J. Peters, T.S. Rushing, E.N. Landis, T.K. Cummins, Nanocellulose and microcellulose fibers for concrete, Transport. Res. Rec. (2142) (2010) 25–28.
- [7] A. Balea, E. Fuente, A. Blanco, C. Negro, Nanocelluloses: natural-based materials for fiber- reinforced cement composites. A critical review, Polymers 11 (3) (2019).
- [8] D. Klemm, et al., Nanocellulose as a natural source for groundbreaking applications in materials science: today's state, Mater. Today 21 (7) (2018).
- [9] H.H. Kolour, M. Ahmed, E. Alyaseen, E.N. Landis, An investigation on the effects of cellulose nanofibrils on the performance of cement paste and concrete, Adv. Civ. Eng. Mater. 7 (1) (2018).
- [10] H.H. Kolour, W. Ashraf, E.N. Landis, Hydration and early age properties of cement pastes modified with cellulose nanofibrils, Transport. Res. Rec. 2675 (9) (2020) 38-46
- [11] O.A. Hisseine, A.F. Omran, A. Tagnit-Hamou, Influence of cellulose filaments on cement paste and concrete, J. Mater. Civ. Eng. 30 (6) (2018) 1–14.
- [12] O. Onuaguluchi, D.K. Panesar, M. Sain, Properties of nanofibre reinforced cement composites, Construct. Build. Mater. 63 (2014) 119–124.
- [13] W. Sekkal, A. Zaoui, Enhancing the interfacial bond strength of cement nanocomposite with carbonate nanostructure, Compos. B Eng. 124 (2017).

- [14] H.P.S. Abdul Khalil, Y. Davoudpour, Md. Nazrul Islam, Asniza Mustapha, K. Sudesh, Rudi Dungani, M. Jawaid, Production and modification of nanofibrillated cellulose using various mechanical processes: a review, Carbohydr. Polym. 99 (2014) 649–665.
- [15] C.J. Chirayil, L. Mathew, S. Thomas, Review of recent research in nano cellulose preparation from different lignocellulosic fibers, Rev. Adv. Mater. Sci. 37 (1–2) (2014)
- [16] P. Phanthong, P. Reubroycharoen, X. Hao, G. Xu, A. Abudula, G. Guan, Nanocellulose: extraction and application, Carbon Resour. Convers. 1 (1) (2018).
- [17] O. Nechyporchuk, M.N. Belgacem, J. Bras, Production of cellulose nanofibrils: a review of recent advances, Ind. Crop. Prod. 93 (2016).
- [18] C. Campano, A. Balea, A. Blanco, C. Negro, Enhancement of the fermentation process and properties of bacterial cellulose: a review, Cellulose 23 (1) (2016).
- [19] L. Zhai, H.C. Kim, J.W. Kim, J. Kang, J. Kim, Elastic moduli of cellulose nanofibers isolated from various cellulose resources by using aqueous counter collision, Cellulose 25 (7) (2018).
- [20] R.J. Moon, A. Martini, J. Nairn, J. Simonsen, J. Youngblood, Cellulose nanomaterials review: structure, properties and nanocomposites, Chem. Soc. Rev. 40 (7) (2011).
- [21] Q. Tarrés, S. Boufi, P. Mutjé, M. Delgado-Aguilar, Enzymatically hydrolyzed and TEMPO-oxidized cellulose nanofibers for the production of nanopapers: morphological, optical, thermal and mechanical properties, Cellulose 24 (9) (2017).
- [22] L. Jiao, M. Su, L. Chen, Y. Wang, H. Zhu, H. Dai, Natural cellulose nanofibers as sustainable enhancers in construction cement, PLoS One 11 (12) (2016).
- [23] S. Parveen, S. Rana, R. Fangueiro, M.C. Paiva, A novel approach of developing micro crystalline cellulose reinforced cementitious composites with enhanced microstructure and mechanical performance, Cement Concr. Compos. 78 (2017).
- [24] J. Goncalves, Y. Boluk, V. Bindiganavile, Cellulose nanofibres mitigate chloride ion ingress in cement-based systems, Cement Concr. Compos. 114 (2020), 103780. August.
- [25] J. Goncalves, M. El-Bakkari, Y. Boluk, V. Bindiganavile, Cellulose nanofibres (CNF) for sulphate resistance in cement based systems, Cement Concr. Compos. 99 (2019) 100–111. March.
- [26] X. Sun, Q. Wu, S. Lee, Y. Qing, Y. Wu, Cellulose nanofibers as a modifier for rheology, curing and mechanical performance of oil well cement, Sci. Rep. 6 (2016).
- [27] Z. Tang, et al., Influence of cellulose nanoparticles on rheological behavior of oilwell cement-water slurries, Materials 12 (2) (2019).
- [28] S. Chakraborty, S.P. Kundu, A. Roy, B. Adhikari, S.B. Majumder, Effect of jute as fiber reinforcement controlling the hydration characteristics of cement matrix, Ind. Eng. Chem. Res. 52 (3) (2013).
- [29] X. Sun, Q. Wu, S. Ren, T. Lei, Comparison of highly transparent all-cellulose nanopaper prepared using sulfuric acid and TEMPO-mediated oxidation methods, Cellulose 22 (2) (2015).
- [30] S. Kawashima, S.P. Shah, Early-age autogenous and drying shrinkage behavior of cellulose fiber-reinforced cementitious materials, Cement Concr. Compos. 33 (2) (2011).
- [31] L.R. Betterman, C. Ouyang, S.P. Shah, Fiber-matrix interaction in microfiber-reinforced mortar, Adv. Cement Base Mater. 2 (2) (1995).
- [32] M. Sarigaphuti, S.P. Shah, K.D. Vinson, Shrinkage cracking and durability characteristics of cellulose fiber reinforced concrete, ACI Mater. J. 90 (4) (1993).
- [33] P. Soroushian, S. Ravanbakhsh, Control of plastic shrinkage cracking with specialty cellulose fibers, ACI Mater. J. 95 (4) (1998).
- [34] N. Buch, O.M. Rehman, J.E. Hiller, Impact of processed cellulose fibers on portland cement concrete properties, Transport. Res. Rec. 1668 (1999).
- [35] J.R. Rapoport, S.P. Shah, Cast-in-place cellulose fiber-reinforced cement paste, mortar, and concrete, ACI Mater. J. 102 (5) (2005).
- [36] B. Mohr, L. Premenko, K. Kurtis, Examination of Wood-Derived Powders and Fibers for Internal Curing of Cement-Based Materials, 2005.
- [37] H.J. Lee, S.K. Kim, H.S. Lee, W. Kim, A study on the drying shrinkage and mechanical properties of fiber reinforced cement composites using cellulose nanocrystals, Int. J. Concr. Struct. Mater. 13 (1) (2019).
- [38] H. Kalhori, R. Bagherpour, Application of carbonate precipitating bacteria for improving properties and repairing cracks of shotcrete, Construct. Build. Mater. 148 (2017).
- [39] M. Shoda, Y. Sugano, Recent advances in bacterial cellulose production, Biotechnol. Bioproc. Eng. 10 (1) (2005).
- [40] N. Reddy, Y. Yang, "Bacterial Cellulose Fibers," in *Innovative Biofibers from Renewable Resources*, 2015.
- [41] P.R. Chawla, I.B. Bajaj, S.A. Survase, R.S. Singhal, Microbial cellulose: fermentative production and applications, Food Technol. Biotechnol. 47 (2) (2009).
- [42] F. Mohammadkazemi, K. Doosthoseini, E. Ganjian, M. Azin, Manufacturing of bacterial nano-cellulose reinforced fiber-cement composites, Construct. Build. Mater. 101 (2015) 958–964.
- [43] E. Cuenca, A. Mezzena, L. Ferrara, Synergy between crystalline admixtures and nano-constituents in enhancing autogenous healing capacity of cementitious composites under cracking and healing cycles in aggressive waters, Construct. Build. Mater. 266 (2021).
- [44] ASTM C150/150M-18, Standard Specification for Portland Cement, Annu. B. ASTM Stand, 2018.
- [45] M.A. Akhlaghi, R. Bagherpour, H. Kalhori, Application of bacterial nanocellulose fibers as reinforcement in cement composites, Construct. Build. Mater. 241 (2020), 118061.

- [46] K.S. Kamasamudram, W. Ashraf, E.N. Landis, Cellulose nanofibrils with and without nanosilica for the performance enhancement of portland cement system, Construct. Build. Mater. 285 (2021), 121547.
- [47] T.F.R. Claramunt J, M. Ardanuy, R. Arevalo, F. Pares, Mechanical performance of ductile cement mortar composites reinforced with nanofibrillated cellulose, *Strain hardening Cem. Compos.*, no. December (2011) 131–138.
- [48] ASTM Committee C09, 26, "ASTM C1260-14 standard test method for potential alkali reactivity of aggregates (mortar-bar method), Annu. B. ASTM Stand. 4.2 (2014) 1–5.
- [49] E.W. Washburn, The dynamics of capillary flow, Phys. Rev. 17 (3) (1921).
- [50] David R. Lide, CRC Handbook of Chemistry and Physics, 84th Edition, 2003-2004, Handb. Chem. Phys., 2003.
- [51] R.A. Cook, K.C. Hover, Experiments on the contact angle between mercury and hardened cement paste, Cem. Concr. Res. 21 (6) (1991).
- [52] S.P. Rigby, New methodologies in mercury porosimetry, in: Studies in Surface Science and Catalysis, vol. 144, 2002.
- [53] J. Kaufmann, R. Loser, A. Leemann, Analysis of cement-bonded materials by multicycle mercury intrusion and nitrogen sorption, J. Colloid Interface Sci. 336 (2) (2009)
- [54] W. Ashraf, J. Olek, N. Tian, Multiscale characterization of carbonated wollastonite paste and application of homogenization schemes to predict its effective elastic modulus, Cement Concr. Compos. 72 (2016) 284–298.
- [55] F. Ulm, M. Vandamme, C. Bobko, J.A. Ortega, Statistical indentation techniques for hydrated nanocomposites: concrete, Bone, and Shale 2692 (2007).
- [56] G. Constantinides, K.S. Ravi Chandran, F.J. Ulm, K.J. Van Vliet, Grid indentation analysis of composite microstructure and mechanics: principles and validation, Mater. Sci. Eng. A 430 (1–2) (2006) 189–202.
- [57] ASTM International, ASTM C109/C109M 20b. Standard test method for compressive strength of hydraulic cement mortars (using 2-in. Or [50 mm] cube specimens), Annu. B. ASTM Stand. 4 (9) (2020).
- [58] American Society for Testing and Materials, Standard Practice for Use of Apparatus for the Determination of Length Change of Hardened Cement Paste, Mortar, and Concrete, ASTM Int., 2011, pp. 1–5.
- [59] M.S. Sajab, et al., Telescopic synthesis of cellulose nanofibrils with a stable dispersion of Fe(0) nanoparticles for synergistic removal of 5-fluorouracil, Sci. Rep. 9 (1) (2019).
- [60] J. Luan, et al., Impregnation of silver sulfadiazine into bacterial cellulose for antimicrobial and biocompatible wound dressing, Biomed. Mater. 7 (6) (2012).
- [61] S. Sepahvand, M. Jonoobi, A. Ashori, F. Gauvin, H.J.H. Brouwers, Q. Yu, Surface modification of cellulose nanofiber aerogels using phthalimide, Polym. Compos. 41 (1) (2020).

- [62] Significance of tests and properties of concrete and concrete-making materials," ASTM (Am. Soc. Test. Mater.) Spec. Tech. Publ., vol. 169 D-STP. 2006.
- [63] F. Rajabipour, E. Giannini, C. Dunant, J.H. Ideker, M.D.A. Thomas, Alkali-silica reaction: current understanding of the reaction mechanisms and the knowledge gaps, Cem. Concr. Res. 76 (2015).
- [64] A. Poole, Introduction to alkali-aggregate reaction in concrete, in: The Alkali-Silica Reaction in Concrete, 1998.
- [65] E.H. Kadri, R. Duval, Effect of Ultrafine Particles on Heat of Hydration of Cement Mortars, ACI Mater. J., 2002.
- [66] W.A. Gutteridge, J.A. Dalziel, Filler cement: the effect of the secondary component on the hydration of Portland cement. Part I. A fine non-hydraulic filler, Cem. Concr. Res. 20 (5) (1990) 778–782.
- [67] B. Lothenbach, K. Scrivener, R.D. Hooton, Supplementary cementitious materials, Cement Concr. Res. 41 (12) (2011).
- [68] J.W. Bullard, et al., Mechanisms of cement hydration, Cement Concr. Res. 41 (12) (2011).
- [69] K.L. Scrivener, A. Nonat, Hydration of cementitious materials, present and future, Cement Concr. Res. 41 (7) (2011).
- [70] I. Pane, W. Hansen, Investigation of blended cement hydration by isothermal calorimetry and thermal analysis, Cem. Concr. Res. 35 (6) (2005).
- [71] K. Scrivener, R. Snellings, B. Lothenbach, A Practical Guide to Microstructural Analysis of Cementitious Materials 62 (10) (1962).
- [72] Y. Cao, et al., The influence of cellulose nanocrystals on the microstructure of cement paste, Cement Concr. Compos. 74 (2016) 164–173.
- [73] W. Ashraf, K. Kamasamudram, K. Kamasamudram, W. Ashraf, and E. Landis, "Construction and Building Materials Cellulose Nanofibrils with and without Nanosilica for the Performance Enhancement of.".
- [74] I. Odler, The BET-specific surface area of hydrated Portland cement and related materials, Cem. Concr. Res. 33 (12) (2003) 2049–2056.
- [75] H.M. Jennings, A. Kumar, G. Sant, Quantitative discrimination of the nano-porestructure of cement paste during drying: new insights from water sorption isotherms, Cem. Concr. Res. 76 (2015) 27–36.
- [76] M.J. Dejong, F. Ulm, The Nanogranular Behavior of C-S-H at Elevated Temperatures (up to 700 ° C), vol. 37, 2007, pp. 1–12. February 2006.
- [77] G. Constantinides, F.J. Ulm, The effect of two types of C-S-H on the elasticity of cement-based materials: results from nanoindentation and micromechanical modeling, Cem. Concr. Res. 34 (1) (2004) 67–80.
- [78] G. Constantinides, F. Ulm, K. Van Vliet, On the Use of Nanoindentation for Cementitious Materials, vol. 36, 2003, pp. 191–196. April.